# Manipulation of Au Spatial Location on TS-1: Enhancement of Catalytic Performance for Direct Propene Epoxidation with $H_2$ and $O_2$

Enhancing Catalytic Performance for Direct Propene Epoxidation with H2 and O2 by engineering of Au Spatial Location on TS-1:

Xiang Feng[†,‡], Zhaoning Song[†], Ketao Zang[‖], Yibin Liu[†], Xiaobo Chen[†], Wenjuan Yan[†], Xin Jin[†], Chaohe Yang[*,†], Jun Luo[‖], De Chen[*,‡] and Xinggui Zhou[*,§]

[†] State Key Laboratory of Heavy Oil Processing, China University of Petroleum, Qingdao, China.
[‡] Department of Chemical Engineering, Norwegian University of Science and Technology, Trondheim, Norway
[§] State Key Laboratory of Chemical Engineering, East China University of Science and Technology, Shanghai, China
[‖] Center for Electron Microscopy, Tianjin University of Technology, Tianjin 300384, China.

**ABSTRACT:** Engineering Au spatial locations on support harbours tremendous potential to boost catalytic performance, but still remains a scientific and technological challenge. Herein, we devise a novel strategy to manipulate Au spatial location on TS-1 support by tuning Au hydrolysis process. By multi-techniques (e.g., quench molecular dynamics simulations, aberration-corrected HAADF-STEM, in-situ UV-vis and model calculation), it is found that slower hydrolysis and different compositions of Au complexes can be achieved using lower temperature. This results in more effective Au clusters near pore mouth of TS-1 microporous channels and smaller-sized Au NPs(using clusters in whole manuscript) on external surfaces. Single Au atoms and Au clusters on Au/TS-1 catalyst are directly observed.necessary? Gratifyingly, the optimum (what is the optimum, or what is the locating ) Au/TS-1 catalyst shows the reported highest initial propylene oxide formation rate without adding promoters and high stable activity for direct propene epoxidation with H2 and O2. Furthermore, overmuch Au clusters inside TS-1 only result in diffusion limit and poor performance, indicating that "effectively accommodated Au clusters" play pivotal role. This strategy offers a promising avenue for the design of efficient Au catalysts by manipulating Au spatial location.

## ■ INTRODUCTION

The discovery that suitably synthesized Au catalyst is catalytically active towards CO oxidation has stimulated extensive work on Au catalysis[1-2]. Well-dispersed Au nanoparticles have been demonstrated to be active for a series of reactions, such as CO oxidation[3-4], selective hydrogenation[5-6], hydrochlorination[6-7], $H_2O_2$ synthesis[8-9] and propene epoxidation[10-11]. Due to the existence of Au size effect, much attention has been focused on reducing Au particle size and even preparing Au sing atoms[4]. It should be noted that these Au atoms, clusters and nanoparticles usually have strong Au-support interaction[10-11], and their locations on support make Au catalysis much more complex. In the past few years, Au spatial location on support is attracting enormous research interests. Take propene epoxidation with $H_2$ and $O_2$ to synthesize propylene oxide (PO) for example, it is a typical structure-sensitive reaction which is the greener, simpler and more sustainable route with higher profit[12-13]. The catalytic performance is highly relevant to the synergy between Au nanoparticles and isolated $Ti^{4+}$-containing supports. It is thus reported that the catalytic performance can be significantly affect by Au particle size[14-15], type of support (e.g., TS-1[11, 13, 16-20], Ti-$SiO_2$[15, 21-22], 3d-titanosilicate[23], TS-1@mesoporous silica[24], Ti-TUD[25], S-1/TS-1[26]), Au location on the internal or external surfaces of support[10], etc. This is mainly because of unique reaction mechanism[14, 20, 27-28] which involves the indispensable roles of both Au and Ti-containing supports. Therefore, the special requirement makes most of Au/Ti-containing catalysts for propene epoxidation prepared by deposition-precipitation (DP) method [14, 17-20, 23-25, 29-38], which could change the Au spatial location (including internal/external surfaces and Ti/Si sites).

DP method is one of the most widely employed methods to prepare well-dispersed Au nanoparticles in Au catalysis[39-43]. By adjusting pH values of preparation process, the support shows distinct electric charges based on the isoelectric point of support[39], and $[AuCl_x(OH)_{4-x}]^-$ could be selectively deposited close to the active titanium sites rather than the inactive silicon sites when the pH of solution is higher than the isoelectric point of silicon sites [20]. Besides the location of Au near Ti species, the Au spatial location also includes Au inside or outside microporous channels of TS-1 support[10, 20]. This usually leads to significantly different catalytic activity and stability. However, few work has reported the strategy to change Au spatial location inside or outside TS-1 microporous channels. There is also no answer on whether it is better to make more Au inside micropores??your paper indicated external is better for stability. Moreover, it is also highly desirable to develop novel strategy to tune Au spatial location, and also to elucidate

the intrinsic interaction between Au spatial location and catalytic performance, which will undoubtedly be beneficial to the rational design of more effective Au catalysts.

In this work, the spatial location of Au inside or outside TS-1 micropores is first manipulated through ~~by~~the Au complex size formed in ~~tuning~~ deposition-precipitation by tuning temperature. The location of the Au on the TS-1 support and formation mechanism are investigated by in-situ UV-vis, aberration-corrected HAADF-STEM, XPS, quench molecular dynamics simulations together with model calculation. Moreover, the underlying structure-performance relationship for propene epoxidation with $H_2$ and $O_2$ is also elucidated. It is found that lower temperature (i.e., 5°C) leads to slower hydrolysis rate and different compositions of Au complexes, resulting in more highly active tiny Au complexes on the internal TS-1 surfaces and smaller-sized Au nanoparticles on external surfaces. For the first time, single Au atoms and Au clusters on Au/TS-1 catalyst are directly observed. Gratifyingly, the 0.10wt% Au/TS-1 catalyst (what is the location) exhibits high initial PO formation rate of 205 $g_{PO}h^{-1}kg_{Cat}^{-1}$, which is almost the reported highest rate without adding promoters. The catalyst also shows higher stable activity. Moreover, the concept of "effectively accommodated Au clusters" inside TS-1 is proposed. Overmuch un-effectively accommodated Au clusters inside TS-1 only result in diffusion limitation and reduced catalytic performance. The insights reported here not only unravel the structure-performance relationship both experimentally and theoretically, but also shed new light on the synthesis of efficient Au catalysts by DP method in a variety of reactions for Au catalysis.

## ■ RESULTS AND DISCUSSION

**Evolution of Au complexes during deposition-precipitation method.** For the deposition-precipitation process of Au precursor (i.e., chloroauric acid), the involved chemistry is mainly about the hydrolysis of $[AuCl_4]^-$ with water to form different Au complexes. Therefore, it can be assumed that at different preparation temperature, the hydrolysis rate should be different. This may lead to distinct Au complexes during synthesis. After reduction, the Au size distribution and Au location (i.e., on the internal or external surfaces of TS-1 support) may also be different, which finally affect the catalytic performance. Therefore, the Au hydrolysis process during deposition-precipitation method is first investigated using UV-vis spectroscopy. Figure 1a shows the UV-vis spectra of Au complexes prepared at different pH. At pH of 2.2, the two bands at ca. 240 and 313 nm are associated with $p_\sigma \rightarrow d_{x^2-y^2}$ and $p_\pi \rightarrow d_{x^2-y^2}$ ligand-to-metal charge transfer transitions from chlorine *p* to gold *d* orbitals, respectively[44-45]. During the progress of Au precursor hydrolysis, the chloride ion is gradually replaced by hydroxyl ion, as shown in equations 2.1-2.4. This leads to the decrease of band intensity together with blue-shift of both bands, which is in consistent with previous results by Baatz[46]. Different Au complexes compositions at each pH value are shown in Table S1 according to literature[47-48].

$$[AuCl_4]^- + H_2O \rightarrow [AuCl_3(OH)]^- + H^+ \quad (2.1)$$

$$[AuCl_3(OH)]^- + H_2O \rightarrow [AuCl_2(OH)_2]^- + H^+ \quad (2.2)$$

$$[AuCl_2(OH)_2]^- + H_2O \rightarrow [AuCl(OH)_3]^- + H^+ + Cl^- \quad (2.3)$$

$$[AuCl(OH)_3]^- + H_2O \rightarrow [Au(OH)_4]^- + H^+ + Cl^- \quad (2.4)$$

Figure 1b illustrates the size and lowest energy configurations of different Au complexes determined by quench molecular dynamic simulation based on literautre[39]. The simulated bond distances of Au-Cl and Au-O are found to be 2.26 Å and 1.88 Å, respectively. They are quite similar to the reported X-ray absorption spectroscopy values of Au-Cl (2.26 Å) and Au-O (1.98 Å) bond distances[49], demonstrating the rationality of simulation. The size of Au complex (*R*) can be calculated as follows: $R = R_{AB} + r_A + r_B$. In this equation, the size of Au complex is equal to the length between two furthest A and B atoms ($R_{AB}$) plus the covalent radii of A ($r_A$) and B ($r_B$) atoms, respectively. The calculated size of $[AuCl_4]^-$ is 6.51 Å,

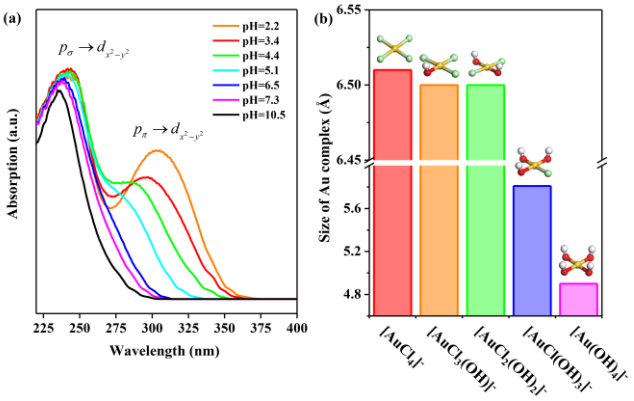


**Figure 1** UV-vis spectra of Au complexes at different pH values (a) and size/structure of Au complexes determined by Quench Molecular Dynamics Simulations (b).

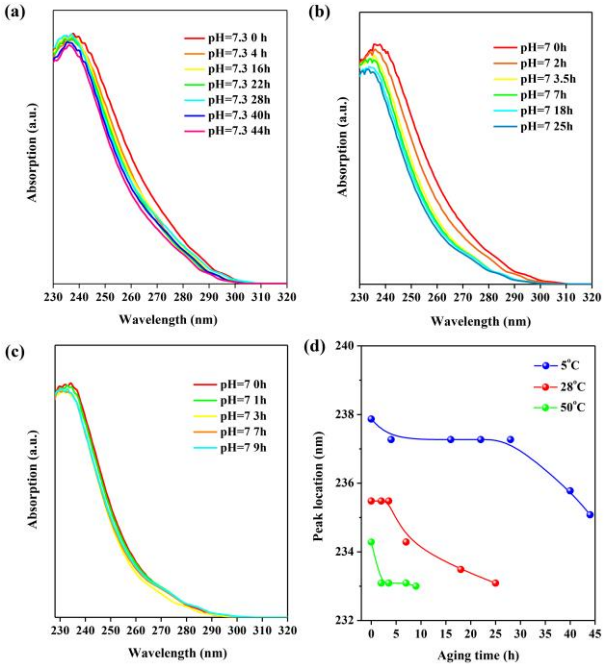


**Figure 2** In-situ UV-vis spectra of Au complexes at different temperature of 5 (a), 28 (b) and 50 °C (c) and the corresponding peak locations at different time-on-stream (d).

slightly larger than that of $[AuCl_3(OH)]^-$ and $[AuCl_2(OH)_2]^-$ with the same size of 6.50 Å. The sizes of $[AuCl(OH)_3]^-$ and

$[Au(OH)_4]^-$ are 5.81 and 4.90 Å, respectively. The decreasing size trend of Au complexes is as follows: $[AuCl_4]^-$ > $[AuCl_3(OH)]^-$ = $[AuCl_2(OH)_2]^-$ > $[AuCl(OH)_3]^-$ > $[Au(OH)_4]^-$. It should be noted that Au complexes with larger molecular size than TS-1 pore size can show stretching and bending vibrations[50-51], and thus could still enter into the micropores of TS-1 supports. In general, the more extensively hydrolyzed Au complexes have higher ability to enter into the micropores of TS-1 due to smaller size and steric hindrance.

Figure 2 shows the in-situ UV-vis spectra of Au complexes as a function of aging time at various preparation time. It is widely accepted that the Au complexes at pH of 7.3-7.5 should include $[AuCl_3(OH)]^-$, $[AuCl_2(OH)_2]^-$, $[AuCl(OH)_3]^-$ and $[Au(OH)_4]^-$.[47-48] From the spectra at different pH (Figure 1a) and detailed Au compositions at different pH in Table S1, the change of Au complexes at different temperature can be expected. For the hydrolysis of Au complexes at room temperature of ca. 28 °C (Figure 2b), there is a slow blue-shift of the main $p_\sigma \rightarrow d_{x^2-y^2}$ band in the initial 18 h and the band keeps slightly changed afterwards. This shows that the hydrolysis is a slow process and long time of ca. 18 h is required to reach hydrolysis equilibrium. In comparison, the hydrolysis process at 5°C (Figure 2a) is much slower than that at 28°C. At 0 h, the Au complexes is already mixed with water (pH is ca. 7) for 30 min, which is mainly designed to represent the real deposition-precipitation process since 30 min is used before the base is added. After 44h, the blue-shift of peak location is still not comparable to that at 28°C, indicating that the Au complexes are still not extensively hydrolyzed. Moreover, it is noted that the peak location is almost unchanged from 4 to 30h, which suggests that the composition of Au complex is not greatly changed due to slow hydrolysis at low temperature. In contrast, the hydrolysis at 50 °C is much more intense, since only 1h is need to reach the extent of blue-shift in comparison to the hydrolysis at 28°C. After 1 h, the peak location is almost unchanged, suggesting that the euqlibrium is almost reached.

**Manipulation of Au location on Au/TS-1 catalyst.** It is already known from literature that Au complexes with different sizes have distinct affinities to the support[52] and thus the abilities of Au complexes into the micropores of TS-1 support are different. In addition, at different hydrolysis temperature, the growth of Au nanoparticles may also be different. Therefore, the physico-chemical properties of TS-1 and Au/TS-1 are subsequently investigated. Figure 3a shows the XRD pattern of TS-1. The presence of a single peak at 24.5° indicates the presence of orthorhombic unit cell. The XRD peaks at 2-theta of 7.9°, 8.8°, 23.1°, 23.9° and 24.5 with high intensity not only coincide with the typical MFI structure of TS-1, but also show high crystallinity of TS-1[43]. Figure 3b displays the $N_2$ adsorption-desorption isotherm of TS-1 support. The microporous characteristic is demonstrated by the typical type I isotherms according to the IUPAC classification[53]. The pore size distribution in the inset of Figure 3b shows that the micropore size of TS-1 is ca. 0.55 nm. With respect to the use of TS-1 in epoxidation reaction, the coordination states of Ti species are one of the most essential parameters. Figure 3c illustrates the FT-IR spectrum of TS-1. The characteristic band of framework Ti species shows up at 960 $cm^{-1}$, indicating the incorporation of titanium into the MFI framework. The adsorption bands at 550 and 1230 $cm^{-1}$ are regarded as vibration of the double five-membered ring unit and asymmetrical stretching vibration of MFI framework structure, respectively[54-55], confirming the XRD results (Figure 3a). Figure 3d shows the UV-vis spectrum of TS-1, and the sharp adsorption peak at 220 nm is the charge transfer from $O^{2-}$ to $Ti^{4+}$ and is ascribed to isolated tetrahedally coordinated Ti[53, 56-57]. This type of $Ti^{4+}$ is indispensable for propene epoxidation[14, 20, 28, 39]. No other adsorption peaks show up at 260 and 330 nm, demonstrating the absence of octahedrally coordinated Ti and anatase phase, respectively.

Au/TS-1 catalysts are then prepared by deposition-precipitation method at different preparation temperature. Figure 4a shows the Au loading as a function of slurry aging time. For Au/TS-1-50C catalyst, Au loading increases from 0.10 to 1.80wt% with the increase of slurry aging time from 1 to 9 h, indicating the high loading rate of Au complexes originated from the intense hydrolysis. In comparison, the Au loading

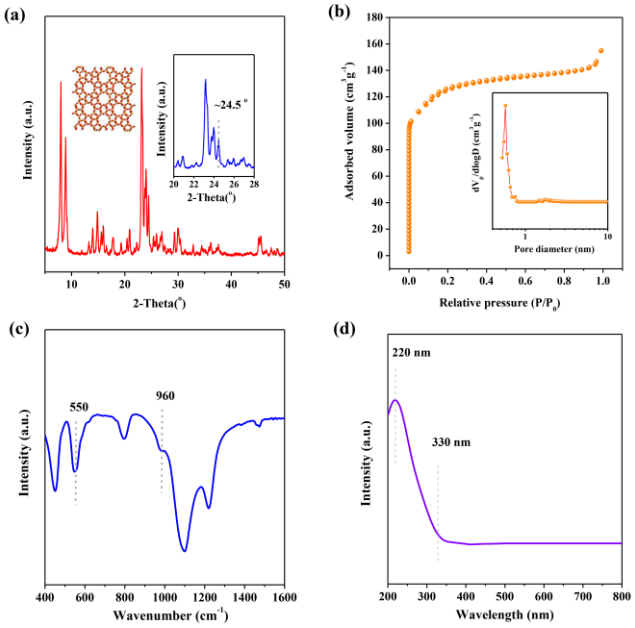


**Figure 3** XRD pattern (a), $N_2$ physisorption (b), FT-IR (c) and UV-vis spectrum (d) of TS-1 support. The inset in Figure 3b shows the pore size distribution.

shows a volcanic-shape relationship with aging time for both Au/TS-1-28C and Au/TS-1-5C catalysts. At 28 °C, Au loading rises from 0.067 to 0.139 wt%, and then decreases to 0.120 wt%. Compared with Au/TS-1-50C catalyst, longer aging time is required for Au/TS-1-28C to get the same Au loading. The reduction of Au loading after 15h aging time can be originated from the affinity between Au complexes and TS-1, as reported by Nechayev et al[52, 58]. It is demonstrated in Figure 2b that the equilibrium is almost reached at 18h. The Au composition at equilibrium shows more extensively hydrolyzed Au complexes (e.g., $[Au(OH)_4]^-$)[48, 52], which have smaller adsorption constant and could be easily removed from TS-1 under vigorous stirring[52, 58]. At lower temperature of 5°C, the slowest loading rate is observed and Au loading reaches the highest value of 0.15wt% at 28 h and then decreases afterwards. During the initial 28h, the Au complexes do not change greatly, as confirmed by in situ UV-vis (Figure 2). However, it can also be seen from Figure 2 that the composition of Au complexes greatly changes after 28h. This leads to the decrease of Au loading on TS-1 support from 0.15 to 0.05wt%. From the above analysis, it can be inferred that the Au loading should be af-

fected by the competition between adsorption rate and removal rate of Au complexes, which are affected by hydrolysis temperature and adsorption ability of Au complexes, respectively. At high temperature, intense hydrolysis dominates and Au loading is not greatly affected by the change of Au adsorption ability since the interaction between Au complex and support is strong. In contrast, at medium and low temperature, the change of Au adsorption ability should dominate, leading to the volcanic-shape relationship between Au loading and slurry aging time.

Figure 4b show the catalytic performance of Au/TS-1 catalysts at different preparation temperature. The linear decrease of PO formation rate is observed for Au/TS-1-50C catalyst, nevertheless, volcanic-shape curves are shown for Au/TS-1-5C and Au/TS-1-28C catalysts. Interestingly, the PO formation rate does not change monotonically with Au loading

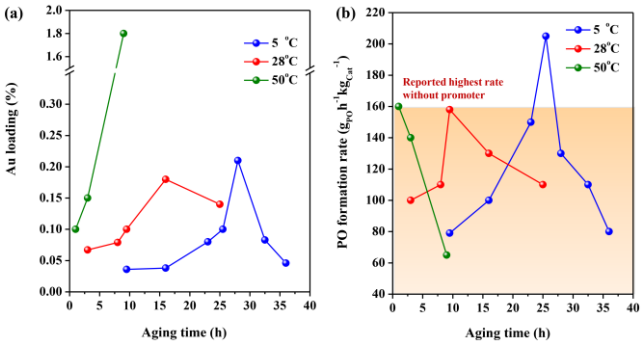


**Figure 4** Au loading (a) and PO formation rate (b) of Au/TS-1 catalysts prepared at different temperature as a function of aging time.

because the optimum PO formation rate for all catalysts have the same loading of 0.10wt%. The highest PO formation rate for propene epoxidation without adding promoters (e.g., Cs) was ca. 160$g_{PO}h^{-1}kg_{Cat}^{-1}$, as reported by Delgass[17]. However, the Au/TS-1-5C catalyst exhibits superior performance of 205 $g_{PO}h^{-1}kg_{Cat}^{-1}$. This enhanced catalytic performance could be mainly affected by the physic-chemical properties of Au nanoparticle and TS-1 support. The TS-1 support is same for all of the Au catalysts. Therefore, the only difference should be related to Au nanoparticles and Au-Ti synergy.

$N_2$ physisorption is subsequently employed to study the Au clusters inside TS-1. As shown in Table 1, the micropore volume of Au/TS-1-5C catalyst reduces from 0.138 to 0.117 $cm^3g^{-1}$ with the increase of aging time from 9.5 to 28 h. In this period, the composition of Au complexes is not greatly changed (Figure 2a), and the Au complexes can gradually enter into the micropores of TS-1, resulting in the reduction of micropore volume. It is also noted that the PO formation rate ($g_{PO}h^{-1}g_{Au}^{-1}$) of Au/TS-1-5C catalysts are almost the same in the same

period, indicating that the Au distribution may be the same due to similar Au complexes. From 28 to 36 h, the micropore volume stops reducing, but rises to 0.134 $cm^3g^{-1}$. This is consistent with the in-situ UV-vis results (Figure 2) and the finding of Nechayev et al. [48] that extensively hydrolyzed Au complexes after a longer aging time could have smaller adsorption constant and be more easily removed from TS-1 under vigorous stirring. Similar phenomenon is also observed for Au/TS-1-28C catalyst. The decreasing trend followed by increasing micropore volume during the 24 h indicates that more extensively hydrolyzed Au complexes first enter into and then move out of the micropores of TS-1. From Figure 2a, Au complexes are different for Au/TS-1-28C catalysts, and thus Au distributions and PO formation rate ($g_{PO}h^{-1}g_{Au}^{-1}$) are different.

**Table 1** Catalyst properties and catalytic performance of different Au/TS-1 catalysts.

| Catalyst | Aging time (h) | Au loading (%) | $D_{Au}$ (nm) | PO formation rate ($g_{PO}h^{-1}g_{Au}^{-1}$) | PO formation rate ($g_{PO}h^{-1}kg_{Cat}^{-1}$) | $V_{MP}$[a] ($cm^3/g$) |
|---|---|---|---|---|---|---|
| TS-1 | N/A | N/A | N/A | N/A | N/A | 0.156 |
| Au/TS-1-5C | 9.5 | 0.037 | 2.3 | 208 | 77 | 0.138 |
| Au/TS-1-5C | 16 | 0.048 | 2.4 | 208 | 100 | 0.134 |
| Au/TS-1-5C | 25 | 0.10 | 2.4 | 205 | 205 | 0.123 |
| Au/TS-1-5C | 28 | 0.15 | 3.5 | 93 | 140 | 0.117 |
| Au/TS-1-5C | 32 | 0.083 | 3.7 | 133 | 110 | 0.119 |
| Au/TS-1-5C | 36 | 0.046 | ND | 174 | 80 | 0.134 |
| Au/TS-1-28C | 4 | 0.067 | 2.7 | 149 | 100 | 0.145 |
| Au/TS-1-28C | 8 | 0.079 | ND | 153 | 120 | 0.140 |
| Au/TS-1-28C | 10 | 0.100 | 3.0 | 160 | 160 | 0.125 |
| Au/TS-1-28C | 18 | 0.139 | 3.2 | 110 | 154 | 0.118 |

| | | | | | | |
|---|---|---|---|---|---|---|
| Au/TS-1-28C | 24 | 0.120 | 3.8 | 89 | 107 | 0.135 |
| Au/TS-1-50C | 1 | 0.10 | 3.2 | 155 | 155 | 0.126 |
| Au/TS-1-50C | 3 | 0.15 | 3.6 | 93 | 140 | 0.116 |
| Au/TS-1-50C | 9 | 1.80 | 4.5 | 4 | 65 | ND |

[a] Micropore volume ($V_{MP}$) is estimated by t-plot method; N/A: Not applicable; ND: Not determined.

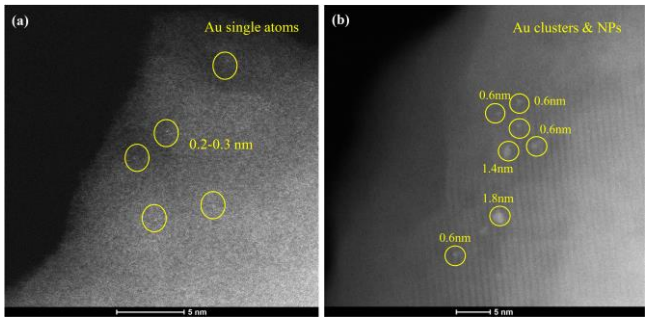


**Figure 5** Aberration-corrected HAADF-STEM images of Au/TS-1-5C catalyst with Au single atoms (a), clusters and nanoparticles (b). The insets shows the particle size distribution and the scale bar represents 5 nm.

The size of Au nanoparticles of Au/TS-1 catalysts at different preparation temperature are first investigated. The observable Au nanoparticle size distribution and average particle size of Au/TS-1-28C by HAADF-STEM are shown in Figure S1. The average Au nanoparticle size is determined as 3.0 nm. It should be noted that the tiny Au clusters inside microporous channels of TS-1 (ca. 0.55 nm) is still not well counted because the aberration-corrected high-angle annular, dark-field scanning transmission with much lower detection limit (ca. 0.07 nm)[59] should be the best choice. Therefore, we further use aberration-corrected HAADF-STEM characterizations. Notably, there indeed exist the Au single atoms (0.2-0.3 nm) and Au clusters confined inside micropores (ca. 0.6 nm). Combined with the decrease of microporous volume, it can be demonstrated that the Au single atoms and clusters can enter into the micropores of TS-1. This is the first direct evidence that these Au species exist on Ti-containing catalysts by DP method since 1998. The averaged Au nanoparticle sizes are shown in Table 1. There is a gradual increase of observable Au particle size with the rise of aging time. At similar Au loading, the Au/TS-1 catalyst prepared at lower DP temperature tends to have smaller observable Au nanoparticle sizes. This is possibly because the slow hydrolysis leads to retarded growth rate of Au crystal. The determined Au particle size is calculated from the observable Au nanoparticles on the external surfaces of TS-1, and Au inside TS-1 are mainly analyzed by the decrease of $V_{MP}$ in Table 1.

In order to better analyze the interaction between Au location and catalytic performance, we introduce two parameters, i.e., $V_{au}$ and $V_{na}$, which are the volume of gold and the volume not accessible to probe molecules ($N_2$). The volume of gold is the weight of gold (i.e., Au loading*0.15g) divided by the gold density (19.3cm³/g). The volume not accessible to $N_2$ is the difference between the micropore volumes of TS-1 support and Au/TS-1 catalyst. If the volume of gold is equal to the volume not accessible to $N_2$, the gold should only cover the sites on TS-1 support and do not leads to blocking phenomenon. In this circumstance, $V_{au}/V_{na}$=1. In contrast, if the volume of gold is smaller than the volume not accessible to $N_2$, some of microporous channels should be blocked by Au nanoclusters, and $V_{au}/V_{na}$<1. If Au block the pore mouth, the $V_{au}/V_{na}$ should be much less than 1. For Au/TS-1-5C and Au/TS-1-28C catalysts, the $V_{au}/V_{na}$ as a function of aging time is shown in Figure 6. It can be seen that both of the two catalysts have very low $V_{au}/V_{na}$, indicating that Au nanoclusters reside into the micropores and lead to the blockage of microporous channels. This is in accordance with the $N_2$ physisorption results. At low aging time, Au nanoclusters tend to first locate at the pore mouth, leading to very small $V_{au}/V_{na}$ of 0.0010 for Au/TS-1-5C. With the increase of aging time, the $V_{au}/V_{na}$ gradually increases and decreases, indicating that more Au clusters enter inside the micropores and gradually move out to pore mouth. This is in accordance with the hydrolysis phenomenon reported by Nechayev et al.[48] Part of Au nanoclusters moving out of the microporous channels of TS-1 to the external surface may lead to the increase of $V_{au}/V_{na}$ again, which could explain the phenomenon between 10-24 h for Au/TS-1-28C catalyst. Interestingly, it is noted that the smaller the $V_{au}/V_{na}$ is, the higher the PO formation is. This could be because Au clusters at pore mouth may show better mass transfer ability[10].

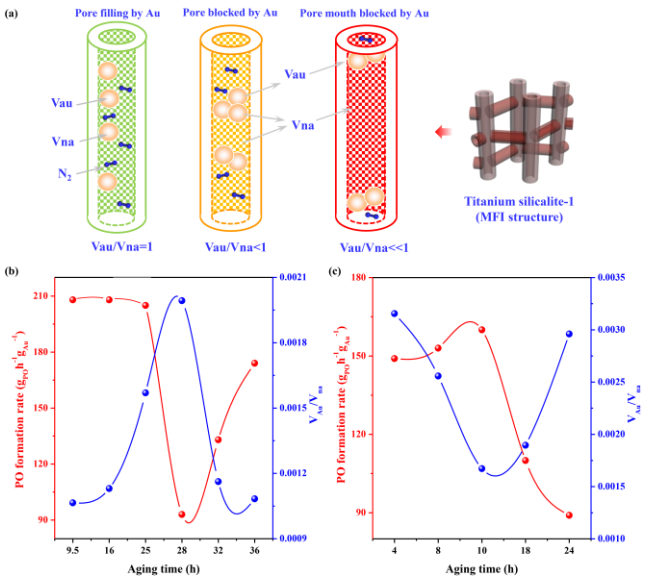


**Figure 6** PO formation rate and $V_{Au}/V_{na}$ as a function of aging time for Au/TS-1-5C (a) and Au/TS-1-28C (b) catalysts.

Based on the Au size effect in propene epoxidation with $H_2$ and $O_2$, the tiny Au clusters inside microporous channels of TS-1 should exhibit higher activity. Therefore, Au/TS-1 with smaller $V_{MP}$ should normally show higher initial PO formation rate. However, it is clearly noted from Table 1 that, the Au/TS-1 catalysts with optimum PO formation rate ($g_{PO}h^{-1}kg_{Cat}^{-1}$) at 5

and 28°C do not show smallest micropore volumes ($V_{MP}$). Herein, the intrinsic reason could be due to the different mass transfer ability inside the micropores of catalyst. Since the space inside TS-1 is limited, an excess of Au complexes inside micropores of TS-1 only lead to diffusion limitation, i.e., part of Au can not be accessible to reactants due to the micropore blocking phenomenon[10, 20] derived from overmuch Au or carbonaceous deposits. Moreover, overmuch Au species inside TS-1 micropores could have limited Ti environment, leading to reduced PO formation rate. The key to enhance catalytic activity seems to be the effectively accommodated Au species inside TS-1 rather than overmuch Au species (Figure 7). As indicated by the results in Figure 6, pore mouth should be one possible scenario for enhancing catalytic performance.

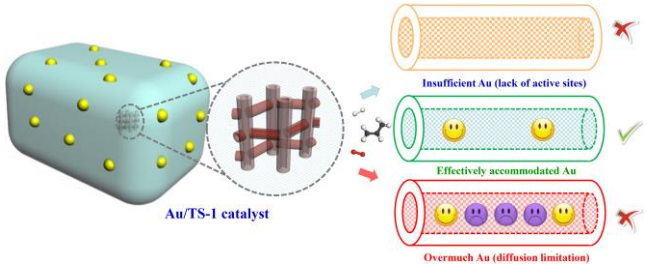


**Figure 7** Schematic diagram of the effectively accommodated Au species in Au/TS-1 catalyst.

**Effect of DP temperature on catalytic performance of 0.10wt% Au/TS-1 catalysts.** To make a fair comparison, Au/TS-1 catalysts prepared at different preparation temperature (5, 28 and 50 °C) with same Au loading of 0.10wt% are compared. The PO formation rates as a function of time-on-stream of Au/TS-1-5C, Au/TS-1-28C and Au/TS-1-50C catalysts are shown in Figure 8a. Compared with Au/TS-1-50C catalyst, impressive PO formation rate of Au/TS-1-5C with a drastic increase from 155 to 205 $g_{PO}h^{-1}kg_{Cat}^{-1}$ is observed. It is known from literature that both external and internal Au are essential for the catalytic performance of Au/TS-1 catalyst[14, 16-17, 20, 38], although internal tiny Au clusters are more active. Figure 8b shows the detailed observable Au nanoparticle size distributions determined from the representative HRTEM images (Figure S2-S4). It can be seen that with the increase of preparation temperature from 5 to 50 °C, the average Au particle size also rises from 2.4 to 3.2 nm, possibly due to faster Au particle growth derived from more intense hydrolysis. The spatial location of Au on the external or internal surfaces of TS-1 can also be investigated by XPS characterization. Table 2 shows the bulk and surface compositions of different Au/TS-1 samples determined by AAS and XPS, respectively. It can be seen that the bulk Au/Si molar ratios of the three catalysts are all smaller than the surface Au/Si molar ratios, demonstrating that Au is not uniformly dispersed on TS-1 support. More Au species tend be located on the external surfaces of TS-1 due to the narrow TS-1 micropores with mass transfer resistance. In addition, it is also noted that the normalized surface Au/Si molar ratio on Au/TS-1-5C catalyst is much smaller than that on Au/TS-1-28C catalyst, indicating that more Au species are located inside TS-1 micropores at 5°C. This is also in accordance with the $N_2$ physisorption results in Table 1. Moreover, the slightly higher normalized surface Au/Si molar ratio on Au/TS-1-50C than Au/TS-1-28C catalyst is also observed.

It is reported that Au/TS-1 catalyst shows Au size-dependence[14] (Figure 8c), and PO formation rate varies with average Au diameter ($d$) as $d^{-2.7\pm0.3}$. Therefore, based on the different external Au size of 0.10wt%Au/TS-1-5C, Au/TS-1-28C and Au/TS-1-50C catalysts, the theoretical PO formation rate ($g_{PO}h^{-1}g_{Au}^{-1}$) if all Au nanoparticles are on external surfaces can be calculated and shown in Figure 8d. Assuming that all Au inside micropores suffer from pore blocking deactivation, the stable activity is thus the PO formation rate of Au on the external surfaces. Therefore, the proportion of Au outside TS-1 micropores can be calculated by dividing the stable PO formation rate by the calculated theoretical PO formation rate. It can be seen that the estimated Au proportion inside of Au/TS-1-5C catalyst is larger than the other two samples. This not only confirm the results of XPS and BET, but also gives a method to calculate the percentage of Au inside micropores.

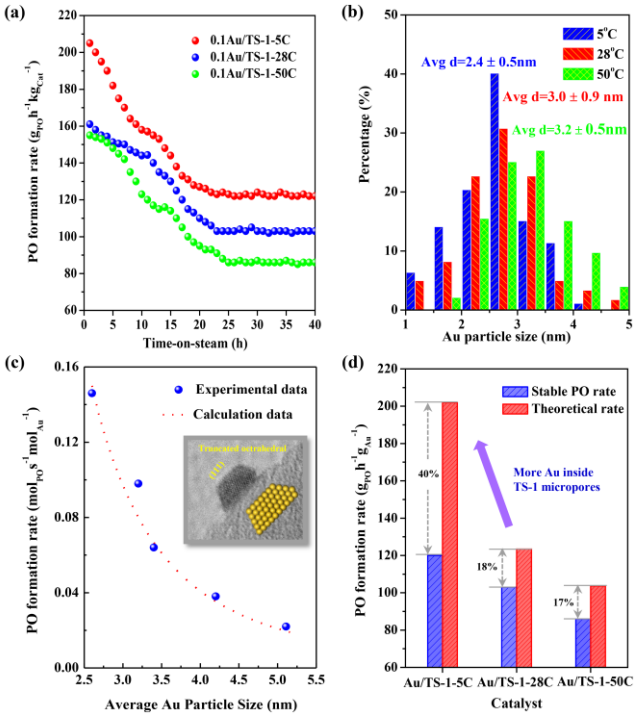


**Figure 8** PO formation rate as a function of time-on-stream (a), Au particle size distribution for different catalysts (b), size-dependent activity (c) and calculated stable PO formation rate for Au/TS-1 catalyst (d).

**Table 2** Bulk and surface Au/Si molar ratios of 0.10wt% Au/TS-1 catalysts.

| Catalyst | Si/Ti ratio | Bulk Au/Si molar ratio (*10$^{-4}$) [a] | Surface Au/Si molar ratio (*10$^{-4}$) [b] | Normalized surface Au/Si molar ratio[c] |
|---|---|---|---|---|
| Au/TS-1-5C | 100 | 3.4 | 3.44 | 0.344 |
| Au/TS-1-28C | 100 | 3.4 | 5.50 | 0.550 |
| Au/TS-1-50C | 100 | 3.4 | 5.64 | 0.564 |

[a] Bulk Au/Si molar ratio is determined by AAS.

[b] Surface Au/Si molar ratio is determined by XPS.

[c] Normalized surface Au/Si molar ratio=(surface Au/Si molar ratio)/(Au loading).

Based on the above analysis, the proportion of Au clusters inside TS-1 micropores follows the trend: Au/TS-1-5C > Au/TS-1-28C > Au/TS-1-50C. Moreover, the catalytic selectivity for each catalyst is shown in Figure 9. The PO selectivities for Au/TS-1-5C, Au/TS-1-28C and Au/TS-1-50C catalysts are 87, 89 and 83%, respectively. For Au/TS-1-5C, Au/TS-1-28C catalysts, the PO selectivities are quite similar. In comparison, the Au/TS-1-50C catalyst has slightly lower PO selectivity, possibly due to larger particle size. The $H_2$ efficiency for Au/TS-1-5C, Au/TS-1-28C and Au/TS-1-50C catalysts are 26, 22 and 20%, respectively. This could be possible due to size effect as reported in our previous reports[39].

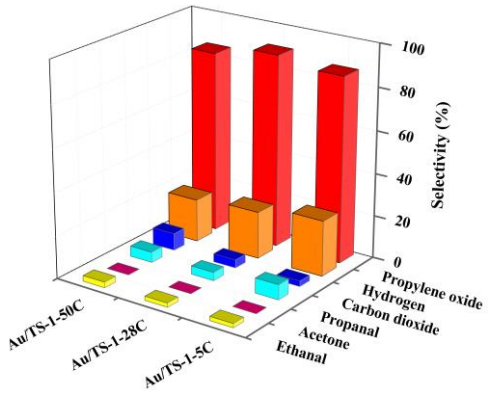


**Figure 9** Selectivity of Au/TS-1-5C, Au/TS-1-28C and Au/TS-1-50C catalysts.

Traditional deposition-precipitation method normally employs room temperature and high temperature (70-90°C) for Au hydrolysis. In this work, it is demonstrated that low temperature delays the hydrolysis rate and also the growth rate of Au crystals on external surfaces of TS-1, allowing more Au clusters to enter inside the micropores of support. Consequently, the as-synthesized Au/TS-1 catalyst exhibits greatly enhanced initial PO formation rate and stable PO formation rate. To the best of our knowledge, this is the reported highest rate without adding promoters (i.e., 205$g_{PO}h^{-1}kg_{Cat}^{-1}$). It should be noted that the "effectively accommodated Au clusters" is emphasized herein. If too much Au clusters reside in the micropores, part of Au clusters deep inside the microspores are not easily accessible by reactants due to diffusional limitation in the narrow microporous channels. Therefore, precise modulation of the "effectively accommodated Au clusters" should be one direction to the enhancement of catalytic performance of Au/TS-1 catalysts in the future. Moreover, it is also observed that the contradiction between high stability and activity still exists since Au clusters inside micropores easily deactivates due to micropore blocking deactivation. However, based on the analysis in this work, it is quite promising to rationally design a novel hierarchical TS-1 support that can not only contains tiny Au clusters inside micropores, but also has better mass transfer ability to inhibit micropore blocking phenomenon. This is an interesting topic and will be carried out in our future work.

## ■ CONCLUSIONS

To sum up, we first devise a new route for the synthesis of effective Au catalyst by low-temperature deposition-precipitation (DP) method, and then elucidate by both theoretical (quench molecular dynamics simulations) and experimental (in-situ UV-vis, HAADF-STEM, XPS, etc.) methods that temperature mainly affect the Au spatial location and also Au particle size. At lower preparation temperature (i.e., 5°C), more Au clusters tend to enter into the micropores of TS-1, and Au nanoparticles on external surfaces of TS-1 are better dispersed (ca. 2.4 nm). As a consequence, the resulted Au/TS-1 catalyst prepared at 5°C shows greatly enhanced PO formation rate of 205 $g_{PO}h^{-1}kg_{Cat}^{-1}$ which is the reported best Au catalysts without adding promoters. For the first time, sing Au atoms and Au clusters on Au/TS-1 catalyst are directly observed, offering a strong evidence that Au could reside into the micropores of TS-1. In addition, the Au clusters lead to blocking of micropores. Effectively accommodated Au clusters inside TS-1 are critical for PO synthesis because too much Au clusters inside TS-1 only result in pore diffusion resistance and reduced catalytic performance. Although preparation temperature can tune the spatial location of Au clusters, more Au species are still on the external surfaces. The stable PO formation also follows the Au size-dependent activity. This finding not only offers a promising avenue for the rational design of highly efficient Au catalysts for propene epoxidation, but also shows considerable influence on improvement of deposition-precipitation method in the fields of Au catalysis.

**Acknowledgments**

This work is financially supported by the Natural Science Foundation of China (21606254), Natural Science Foundation of Shandong Province (ZR2016BB16), Key research and development plan of Shandong Province (2017GSF17126), Fundamental Research Funds for the Central Universities (18CX02014A) and Independent innovation foundation of Qingdao (17-1-1-18-jch).

## ■ EXPERIMENTAL SECTION

**Synthesis of TS-1 supports and different Au/TS-1 catalysts.** Microporous Titanium silicalite-1 (TS-1) supports with Si/Ti molar ratio of 100 was synthesized according to classical hydrothermal method[17, 43]. In a typical process, 3.5 g tween-20 was added to 45 mL deionized water, and the solution was added to the mixture of 44.8 g tetrapropylammonium hydroxide (TPAOH, 25 wt%) and 66.4 g tetraethylorthosilicate (TEOS, 95 wt%). The solution was stirred at 28°C for more than 30 min. Subsequently, titanium (IV) tetrabutoxide (TBOT, 99 wt%) dissolved in 20 mL isopropanol (WAKO, 99.5 wt%) was then added drop-wise to avoid the formation of $TiO_2$. The final solution containing template, Ti and Si source was further stirred for more than 1 h and crystallized in a Teflon autoclave at 170°C for more than 18 h. The as-obtained uncalcined TS-1 was thoroughly washed and dried overnight at room temperature. This is followed by calcination at 550°C for 5.5 h.

Au/TS-1 catalysts were prepared by the deposition-precipitation (DP) method as outlined in our previous reports[14, 20, 28] with different preparation temperatures. 0.5 g TS-1 was first mixed with 0.1 g $HAuCl_4 \cdot 3H_2O$ and 50 mL $H_2O$ for 30 min at different temperatures (i.e., 5, 28, 50°C). The pH of Au precursor and TS-1 slurry was adjusted to 7.3-7.5 by 1 M and 0.1 M NaOH and then aged for different hours to tune Au loadings. The solid was then centrifuged, washed and dried at 28 °C under vacuum. The as-prepared Au/TS-1 catalyst prepared at *x* °C is denoted as Au/TS-1-*x*C catalyst. For example, Au/TS-1-5C represents Au/TS-1 catalyst prepared at 5°C.

**Characterization and quench molecular dynamics simulation.** X-ray diffraction (XRD, Rigaku D/Max2550VB/PC, Cu $K_\alpha$ radiation) was used to characterize the crystal phases of the

TS-1 supports. In situ ultraviolet-visable spectroscopy was recorded on a spectrometer (AvaSpec-2048) equipped with a transmission dip probe in order to determine the Au complexes. $N_2$ physisorption (Micromeritics ASAP 2020) was taken to measure the pore diameters and pore volumes of the Au/TS-1 catalysts prepared at different temperature. Atomic absorption spectroscopy (AAS, ZEEnit 600) was employed to determine weight percentages of elements. High-angle annular dark-field scanning transmission electron microscopy (HAADF-STEM) was performed on a Tecnai G2 F20 S-Twin equipped with a digitally processed STEM imaging system. More than 150 nanoparticles were counted to make an accurate Au particle size distribution. X-ray photoelectron spectroscopy (XPS) on a Kratos XSAM-800 instrument using Al $K_\alpha$ X-ray with 1486.6 eV as the excitation source was used to give the surface Au/Si molar ratios.

Stable structures of Au complexes with the lowest energy conformation were obtained by quench molecular dynamics simulation using Materials Studio package. The UFF (Universal Force Field) was used and the simulation was conducted at 298 K in the microcanonical ensemble (NVE). The time step and total simulation time were set as 1 fs and 100 ps, respectively. Geometry optimization calculations were performed every 5 ps.

**Catalytic testing.** Direct gas-phase propene epoxidation with $H_2$ and $O_2$ was carried out in a quartz tubular reactor (i.d. 8 mm) using 0.15 g catalyst of 60-80 mesh particle size at 1 bar. The reactor was heated from room temperature to 200 °C with $C_3H_6$, $H_2$, $O_2$ and $N_2$ of 10/10/10/70 vol.%, respectively. The feedstock was fixed at a space velocity of 14,000 $mL h^{-1} g_{cat}^{-1}$. The concentration of reactants ($C_3H_6$, $H_2$ and $O_2$) and products (PO, $CO_2$, acetaldehyde, acetone, propanal, acrolein and so on) were measured online by two gas chromatographs (Agilent 6890) equipped with TCD (Porapak Q and 5A columns) and FID (Porapak T column) detectors. The carbon balance, conversion and selectivity were defined as follows:

Carbon balance = (3×(propene + PO + Propanal + Acetone) + 2×ethanal+$CO_2$) / (3×propene)

Propene conversion = moles of ($C_3$-oxygenates + 2/3ethanal + $CO_2$/3)/moles of propylene in the feed.

$H_2$ conversion = moles of $H_2$ converted/moles of $H_2$ in the feed.

$C_3$-oxygenate selectivity = moles of $C_3$-oxygenate/moles of ($C_3$-oxygenates + 2/3ethanal + $CO_2$/3).

Ethanal selectivity = 2/3(mole of ethanal)/moles of ($C_3$-oxygenates + 2/3ethanal + $CO_2$/3).

$H_2$ efficiency = moles of PO/moles of $H_2$ converted.

It should be noted that the $CO_2$ can be well-analyzed in this work, and carbon balance is larger than 95%.

## ■ ASSOCIATED CONTENT

Supporting Information. Representative HRTEM image of catalysts and The composition of Au complexes at different pH levels. This material is available free of charge via the Internet at http://pubs.acs.org.

## ■ AUTHOR INFORMATION

### Corresponding Author

* De Chen: de.chen@ntnu.no
* Xinggui Zhou: xgzhou@ecust.edu.cn
* Chaohe Yang: yangch@upc.edu.cn

## ■ ACKNOWLEDGMENT

The present work was financially supported by the Natural Science Foundation of China (21606254), Natural Science Foundation of Shandong Province (ZR2016BB16), Key research and development plan of Shandong Province (2017GSF17126), Fundamental Research Funds for the Central Universities (18CX02014A) and Independent innovation foundation of Qingdao (17-1-1-18-jch).

## ■ REFERENCES

1. Haruta, M.; Kobayashi, T.; Sano, H.; Yamada, N. *Chem. Lett.* **1987,** *16* (2), 405-408.
2. Okumura, M.; Fujitani, T.; Huang, J.; Ishida, T. *ACS Catal.* **2015,** *5* (8), 4699-4707.
3. Saavedra, J.; Doan, H. A.; Pursell, C. J.; Grabow, L. C.; Chandler, B. D. *Science* **2014,** *345* (6204), 1599-1602.
4. Wang, Y.; Widmann, D.; Behm, R. J. *ACS Catal.* **2017,** *7* (4), 2339-2345.
5. Aguilar-Tapia, A.; Delannoy, L.; Louis, C.; Han, C. W.; Ortalan, V.; Zanella, R. *J. Catal.* **2016,** *344*, 515-523.
6. Masoud, N.; Delannoy, L.; Calers, C.; Gallet, J.-J.; Bournel, F.; de Jong, K. P.; Louis, C.; de Jongh, P. E. *ChemCatChem* **2017,** *9* (12), 2418-2425.
7. Zhou, K.; Jia, J.; Li, C.; Xu, H.; Zhou, J.; Luo, G.; Wei, F. *Green Chem.* **2015,** *17* (1), 356-364.
8. Yang, X.J.; Tian, P.F.; Wang, H.L.; Xu, J.; Han, Y.F. *J. Catal.* **2016,** *336*, 126-132.
9. Zheng, Z.; Ng, Y. H.; Wang, D.W.; Amal, R. *Adv. Mater.* **2016,** *28* (45), 9949-9955.
10. Feng, X.; Liu, Y.; Li, Y.; Yang, C.; Zhang, Z.; Duan, X.; Zhou, X.; Chen, D. *AIChE J.* **2016,** *62* (11), 3963-3972.
11. Feng, X.; Sheng, N.; Liu, Y.; Chen, X.; Chen, D.; Yang, C.; Zhou, X. *ACS Catal.* **2017,** *7* (4), 2668-2675.
12. Hayashi, T.; Tanaka, K.; Haruta, M. *J. Catal.* **1998,** *178* (2), 566-575.
13. Huang, J.; Takei, T.; Akita, T.; Ohashi, H.; Haruta, M. *Appl. Cataly. B: Environ.* **2010,** *95* (3–4), 430-438.
14. Feng, X.; Duan, X.; Qian, G.; Zhou, X.; Chen, D.; Yuan, W. *J. Catal.* **2014,** *317*, 99-104.
15. Qi, C.; Huang, J.; Bao, S.; Su, H.; Akita, T.; Haruta, M. *J. Catal.* **2011,** *281* (1), 12-20.
16. Huang, J.; Lima, E.; Akita, T.; Guzmán, A.; Qi, C.; Takei, T.; Haruta, M. *J. Catal.* **2011,** *278* (1), 8-15.
17. Lee, W.S.; Cem Akatay, M.; Stach, E. A.; Ribeiro, F. H.; Nicholas Delgass, W. *J. Catal.* **2012,** *287* (0), 178-189.
18. Lee, W.S.; Cem Akatay, M.; Stach, E. A.; Ribeiro, F. H.; Nicholas Delgass, W. *J. Catal.* **2013,** *308*, 98-113.
19. Lee, W.S.; Cem Akatay, M.; Stach, E. A.; Ribeiro, F. H.; Nicholas Delgass, W. *J. Catal.* **2014,** *313* (0), 104-112.
20. Feng, X.; Duan, X.; Qian, G.; Zhou, X.; Chen, D.; Yuan, W. *Appl. Catal. B: Environ.* **2014,** *150*, 396-401.
21. Chen, J.; Halin, S. J.; Pidko, E. A.; Verhoeven, M.; Ferrandez, D. M. P.; Hensen, E. J.; Schouten, J. C.; Nijhuis, T. A. *ChemCatChem* **2013,** *5* (2), 467-478.
22. Qi, C. *Gold Bulletin* **2008,** *41* (3), 224-234.
23. Sinha, A. K.; Seelan, S.; Tsubota, S.; Haruta, M. *Angew. Chem. Inter. Ed.* **2004,** *43* (12), 1546-1548.
24. Xu, L.; Ren, Y.; Wu, H.; Liu, Y.; Wang, Z.; Zhang, Y.; Xu, J.; Peng, H.; Wu, P. *J. Mater. Chem.* **2011,** *21* (29), 10852-10858.
25. Lu, J.; Zhang, X.; Bravo-Suárez, J. J.; Bando, K. K.; Fujitani, T.; Oyama, S. T. *J. Catal.* **2007,** *250* (2), 350-359.
26. Li, Z.; Zhang, J.; Wang, D.; Ma, W.; Zhong, Q. *J. Phys. Chem. C* **2017,** *121* (45), 25215-25222.
27. Bravo-Suarez, J. J.; Bando, K. K.; Lu, J.; Haruta, M.; Fujitani, T.; Oyama, T. *J. Phys. Chem. C* **2008,** *112* (4), 1115-1123.

28. Feng, X.; Duan, X.; Yang, J.; Qian, G.; Zhou, X.; Chen, D.; Yuan, W. *Chemical Engineering Journal* **2014**, 278,234-239.
29. Yang, H.; Tang, D.; Lu, X.; Yuan, Y. *J. Phys. Chem. C* **2009,** *113* (19), 8186-8193.
30. Qian, G.; Yuan, Y. H.; Wu, W.; Zhou, X. G. *Stud Surf Sci Catal*. **2006**, 159, 333-336.
31. Yuan, Y.H.; Zhou, X.G.; Wu, W.; Zhang, Y.R.; Yuan, W.K.; Luo, L. *Catal. Today* **2005,** *105* (3–4), 544-550.
32. Sinha, A. K.; Seelan, S.; Akita, T.; Tsubota, S.; Haruta, M. *Appl. Catal. A: Gen.* **2003,** *240* (1–2), 243-252.
33. Uphade, B. S.; Akita, T.; Nakamura, T.; Haruta, M. *J. Catal.* **2002,** *209* (2), 331-340.
34. Mul, G.; Zwijnenburg, A.; van der Linden, B.; Makkee, M.; Moulijn, J. A. *J. Catal.* **2001,** *201* (1), 128-137.
35. Nijhuis, T. A.; Huizinga, B. J.; Makkee, M.; Moulijn, J. A. *Ind. Eng. Chem. Res.* **1999,** *38* (3), 884-891.
36. Du, M.; Zhan, G.; Yang, X.; Wang, H.; Lin, W.; Zhou, Y.; Zhu, J.; Lin, L.; Huang, J.; Sun, D.; Jia, L.; Li, Q. *J. Catal.* **2011,** *283* (2), 192-201.
37. Chen, J.; Pidko, E. A.; Ordomsky, V. V.; Verhoeven, T.; Hensen, E. J.; Schouten, J. C.; Nijhuis, T. A. *Catal. Sci. Tech.* **2013,** *3* (11), 3042-3055.
38. Lee, W.S.; Lai, L.C.; Cem Akatay, M.; Stach, E. A.; Ribeiro, F. H.; Delgass, W. N. *J. Catal.* **2012,** *296* (0), 31-42.
39. Feng, X.; Duan, X.; Cheng, H.; Qian, G.; Chen, D.; Yuan, W.; Zhou, X. *J. Catal.* **2015,** *325*, 128-135.
40. Hugon, A.; El Kolli, N.; Louis, C. *J. Catal.* **2010,** *274* (2), 239-250.
41. Lu, X.; Zhao, G.-F.; Lu, Y. *Catal. Sci. Technol.* **2013**, 3:2906-2909.
42. Moreau, F.; Bond, G. C.; Taylor, A. O. *J. Catal.* **2005,** *231* (1), 105-114.
43. Khomane, R. B.; Kulkarni, B. D.; Paraskar, A.; Sainkar, S. R. *Mater Chem Phys.* **2002,** *76* (1), 99-103.
44. Gangopadhayay, A. K.; Chakravorty, A. *J. Chem. Phys.* **2004,** *35* (6), 2206-2209.
45. Peck, J. A.; Tait, C. D.; Swanson, B. I.; Brown Jr, G. E. *Geochim. Cosmochim. AC.* **1991,** 55 (3), 671-676.
46. Baatz, C.; Decker, N.; Prüße, U. *J. Catal.* **2008,** *258* (1), 165-169.
47. Moreau, F.; Bond, G. C. *Catal. Today* **2007,** *122* (3–4), 260-265.
48. Nechayev, Y. A.; Nikolenko, N. *Geochem. Int.* **1986,** *23*, 142-146.
49. Chen, X.; Chu, W.; Chen, D.; Wu, Z.; Marcelli, A.; Wu, Z. *Chem. Geol.* **2009,** *268* (1–2), 74-80.
50. Schmidbaur, H.; Raubenheimer, H. G.; Dobrzańska, L. *Chem. Soc. Rev.* **2014,** *43* (1), 345-380.
51. Maity, M.; Das, S.; Maiti, N. C. *Phys. Chem. Chem. Phys.* **2014,** *16* (37), 20013-20022.
52. Lee, S.-J.; Gavriilidis, A. *J. Catal.* **2002,** *206* (2), 305-313.
53. Wang, Z.; Xu, L.; Jiang, J.G.; Liu, Y.; He, M.; Wu, P. *Microporous Mesoporous Mater.* **2012,** *156*, 106-114.
54. Wu, P.; Tatsumi, T.; Komatsu, T.; Yashima, T. *J. Phys. Chem. B.* **2001,** *105* (15), 2897-2905.
55. Zecchina, A.; Bordiga, S.; Lamberti, C.; Ricchiardi, G.; Scarano, D.; Petrini, G.; Leofanti, G.; Mantegazza, M. *Catal. Today* **1996,** *32* (1), 97-106.
56. Serrano, D.; Sanz, R.; Pizarro, P.; Moreno, I.; Medina, S. *Appl. Catal. B: Environ.* **2014,** *146*, 35-42.
57. Duprey, E.; Beaunier, P.; Springuel-Huet, M. A.; Bozon-Verduraz, F.; Fraissard, J.; Manoli, J.M.; Brégeault, J. M. *J. Catal.* **1997,** *165* (1), 22-32.
58. Nechayev, Y. A.; Nikolenko, N. *Geochem. Int.* **1986,** *23*, 142-146.
59. Yang, M.; Li, S.; Wang, Y.; Herron, J. A.; Xu, Y.; Allard, L. F.; Lee, S.; Huang, J.; Mavrikakis, M.; Flytzani-Stephanopoulos, M. *Science* **2014,** *346* (6216), 1498-1501.

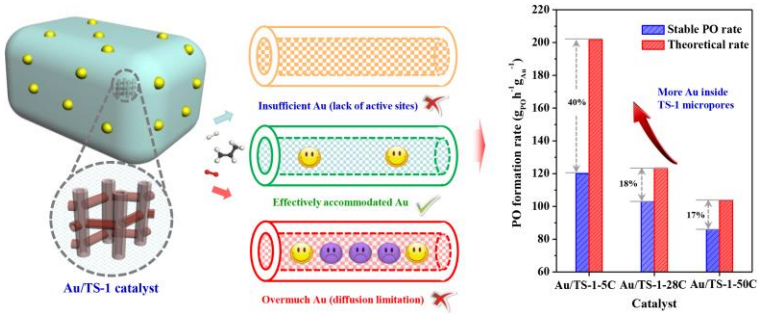


Table of Contents